The 2010 IEEE/RSJ International Conference on
Intelligent Robots and Systems
October 18-22, 2010, Taipei, Taiwan

Probabilistic Landmark Based Localization of Rail Vehicles in Topological Maps

Stefan Hensel and Carsten Hasberg

Abstract— **Localization of rail vehicles is fundamental for any autonomous systems to perform tasks in logistics or personal transport. This contribution presents a novel onboard localization system, based on an eddy current sensor system (ECS), that is capable of a precise train localization when combined with a simple topological map. In contrary to commonly applied travel distance determination by integrating the estimated velocity, we propose an event triggered counting approach, which makes use of the unique sensor capabilities. Rail switches are chosen as landmarks for a global map association and as reliable start and end points for the counting procedure. They are extracted via a Bayesian filter approach, in particular hidden Markov models are applied for detection and classification. Additional features are modeled in a subsequent step and merged within a topological map employing a naïve Bayesian approach in the spatial domain. This allows for a flexible sensor integration and an easy determination of the most probable vehicle position based on traveled distanced.**

I. Introduction

Autonomous rail vehicles are restricted to production lines or closed marine facilities at present. Potential fields of application are logistics, ore transportation in mining sites [1], and side track networks for local passenger transportation in flexible transportation units [2].

Current rail vehicle localization systems are either based upon track side infrastructure installations, positioning with global navigation satellite systems (GNSS) [3], or a combination of both [4]. One drawback of these approaches is the relatively low accuracy of odometrial measurements, usually implemented with inductive rev-counters. Even the GNSS speed and position information is often too inaccurate taken into account that rail side tracks are commonly situated either in industrial areas, forests or valleys with dense vegetation and comprise additional obstacles such as tunnels and station halls.

Localization in robotics is often based on accurate geometrical maps [5]. Autonomous rail vehicles are not to leave the tracks, and thus represent a one dimensional motion conditioned on the track. We propose to use topological maps to solve the localization. They are well examined and applications can be found in [6] or [7], whereas geometric maps for rail networks are scarcely available and expensive in creation, especially for side tracks. Topological network plans are well established in contrary, e.g. metro plans or schemata at train control centers. If not available, a rough drawing is trivially done by any person that knows the track [7]. Besides their availability and easy creation topological maps expose an efficient and natural way of depicting the environment [8].

Yet, there are two main problems, that must be solved to achieve a reliable localization within the maps. Determination of the current track segment is necessary for any global assignment and the estimation of the position upon that segment is needed for local accuracy. We propose a system solely based on a novel eddy current sensor (ECS). The sensor system is capable of a slipless and hence precise velocity estimation and the detection of common track features, e.g. turnouts or bridges. The latter can be used to distinguish discrete intervals on rail tracks separated by sleeper clamps. Our contribution focuses on this discrete distance information, i.e. the traveled distance is determined by sleeper counting techniques. We show that this approach is better suited for longer distances between two landmarks, which mainly occurs in autonomous mining transports and side track logistics. This is in contrast to odometrial techniques, better suited for areas with a high turnout density [9].

The whole localization is thus performed in relative distance units, initialized on distinctive turnouts that represent landmarks defining the topological edges. We apply probabilistic methods for landmark detection, classification, and information fusion in the map to cope with misclassification noisy measurements, and partly incorrect a priori information. Advantages of this stochastic concept are impressively shown in many robotics [5], [8], tracking [10] and machine learning [11] applications. The Bayesian framework we employ for turnout extraction and map based localization is intuitive, robust, and easy augmentable. For the successive fusion, the measurements can arrive in different frequency and represent landmarks or edge features.

The remainder of the paper is organized as follows: Section II will introduce the eddy current sensor system and how it is applied for estimation of discrete distance information. Pattern recognition with hidden Markov models is object of Section III. It is shown how probabilistic models can be employed to detect and continuously extract turnouts and subsequently classify the extracted samples. Distance and turnout information are combined within the map, which is subject of Section IV. An overall overview with interdependencies of the system is given in Fig. 1 for clarification.

II. Eddy Current Sensor System (ECS)

Eddy current sensors are used to detect inhomogeneities in the magnetic resistance of ferromagnetic materials. The presented system consists of two differential sensors in a

S. Hensel and C. Hasberg are with institute of Measurement and Control, Karlsruhe Institute of Technology, 76131 Karlsruhe, Gernmany {hensel, hasberg}@mrt.uka.de

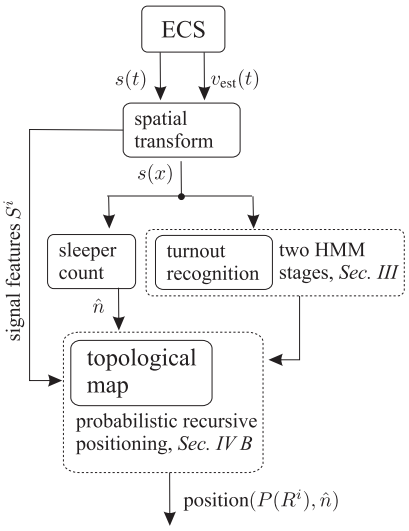

Fig. 1. Blockdiagram of proposed localization algorithm.

row, separated by the distance l. The sensors are placed in a housing for electromagnetical shielding, which is mounted 100 mm above the railhead of the train bogie. This enables the sensor to detect all major changes in the magnetic field along the track, mainly rail clamps but also turnouts and their components. The theoretical signal $s_1(x)$ of one differential sensor is shown in Figure 2 a). The ECS has

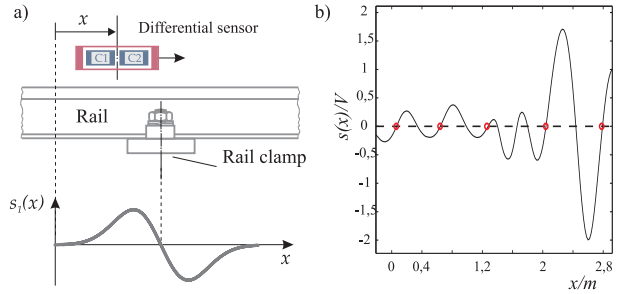

Fig. 2. a) Ideal spatial signal $s_1(x)$ of one differential sensor, built up of two coils $C1$ and $C2$ when crossing an inhomogeneities. b) Valid zero crossings in a given signal. The crossings are marked with circles, crossings too close together are rejected due to prior knowledge.

two measurement outputs: The velocity v_{est}, calculated with a closed loop correlator (CLC, see [12]) based on cross correlation techniques and a subsequent fusion in a Kalman Filter (see [13] for further details), given the coil distance l. The second are raw signals $s_1(t)$ and $s_2(t)$ of each sensor. On open tracks, it is mainly induced by the clamps, whose equidistant spacing yields an almost periodic signal. A considerable change of the signal, mainly in amplitude, is observable when the sensor enters turnout areas, bridges or comparable regions.

A. Distance Measurement

Prerequisite for event detection is a spatial signal $s(x)$ transformed from one of the original time signals $s_1(t)$ or $s_2(t)$ and the estimated velocity v_{est}, with $\hat{x}(t) = \int_0^t v_{\text{est}}(\tau)d\tau$. The remainder of the paper uses $s(x)$ instead $s_{1,2}(\hat{x})$, whereas the second channel can be used for redundancy and measurement uncertainty taken into mind. Figure 3 shows exemplary real data signals. To avoid wrong counting in turnout areas (as seen in the middle of Figure 3) a bandpass filter is applied to the signal. The band is chosen around the main sleeper frequency $f_{\text{sl}} = 1.5\frac{1}{\text{m}}$ for open track areas. Given this information, one can estimate the sleeper number even in bad signal to noise conditions that appear in low speed maneuvers as depicted in the right plot in Figure 3. Utilizing that every sleeper induces two zero crossings, we apply a signum transform and consecutive search of the falling flank. In addition, using spatial signal properties, peaks too close together are rejected. Results for this algorithm are shown in Figure 2 b). The number of sleepers $n_{\text{sl}}(t)$ at a specific time t can be used for an incremental distance measurement that is free of integrative drift. Nonetheless, one must cope with counting errors. The sleeper count distance is discrete with

$$\hat{d}_{\text{sl}}(t) = \sum_{i=1}^{n_{\text{sl}}(t)} \Delta n_i, \tag{1}$$

which implies a minimum error of $\Delta n = 0.65\text{m}$. Given this average space between two sleepers the error becomes significantly smaller than integrative distance measures, the longer the measured distance between two points. This approach is therefore especially useful on side tracks, e.g. heavy transport routes, with only few stations.

III. Turnout Extraction and Classification

To sensibly count the sleepers, a reliable start and end point determination is needed, as mentioned before. This is realized by identifying turnouts within the signal. Because they are also the natural choice for nodes in a topological map, they represent landmarks, useful for global positioning and counter resets.

A. Hidden Markov Models

Besides noise and amplitude changes due to bogie movements and external influences like temperature gradients, exists a vast diversity of turnouts different in type, size and specific local features. To cope with this variety a stochastic, model based approach with hidden Markov models (HMMs) is applied to localize the turnouts and separate them from other track specific features.

Each HMM is completely determined by its parameter set $\boldsymbol{\lambda} = (\boldsymbol{\pi}, \mathbf{A}, \mathbf{B})$. Where $\boldsymbol{\pi}$ is the initial probability vector, $\mathbf{A}$ the *transition matrix* and $\mathbf{B}$ the *emission matrix*, containing information for the parameterized emission densities. Further information on HMMs can be found in [14].

B. Turnout Segmentation

Again, the transformed signal $s(x)$ is basis for any turnout extraction. Afterwards, the stochastic model is built based upon an ideal turnout shown in Figure 4, which also depicts an exemplarily ECS signal of a turnout. It illustrates the different amplitudes and shapes of the signal when passing

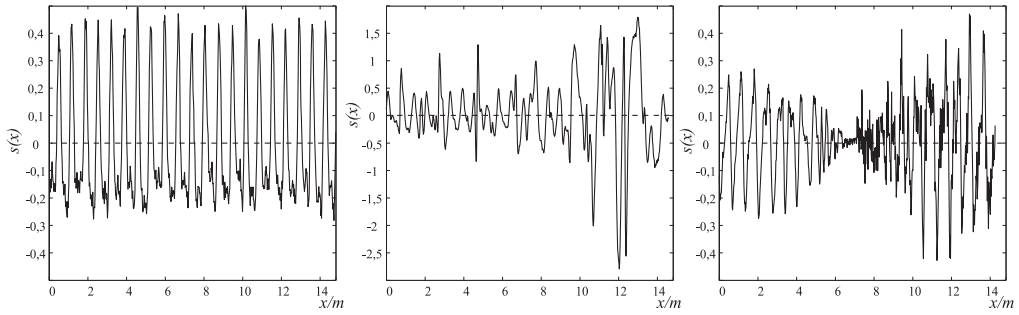

Fig. 3. Examples of ECS signals. They depict from left to right: Common rail clamp signals, rail guard of a turnout and filter effects when decelerating to and accelerating from stand still.

turnouts. Each physical segment, e.g. frog, represents a state of the HMM. This allows a validation of the segmented results by evaluating the state duration and probability characteristics of the estimated *a posteriori* sequence. To obtain

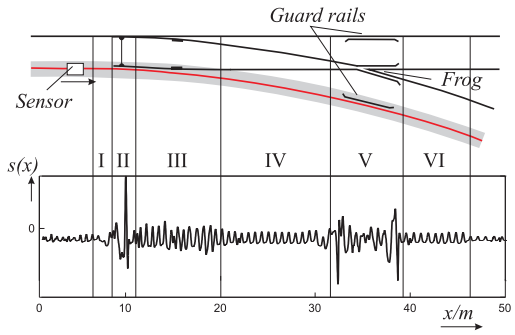

Fig. 4. Scheme of a turnout and corresponding sensor signal $\tilde{r}(l)$ when driving on the right branch track.

a non-periodic signal, the envelope of the power signal is computed via Hilbert transformation (see [15]). This signal represents the input for the segmentation HMM. The parameters of the emission matrix are determined with maximum likelihood estimation of real ECS signals using Gaussian distributions. The transition probabilities and, therefore, implicitly the state durations of the HMM are modeled with the *state-tying* technique [14] to transform the intrinsic geometric distribution to the negative binomial distribution. This allows to set position and precision of the binomial modes to represent the length of the turnout components. Turnout parts with high discriminative character, such as guard rails or switchblades contain more sub states, while interconnecting areas are built up of few sub states to catch up with the different length of the several turnout types.

The resulting HMM consists of six sub models $\boldsymbol{\lambda}_{1..6}$ that represent the four possible turnout passing directions and two models for disturbances such as bridges, cables or accidentally placed metal parts, e.g. tin cans. The six models are interconnected by an additional bimodal sleeper state to enable continuous signal segmentation. Evaluation is performed with the Viterbi algorithm according to [11]. The path is continuously computed with a moving window length varying from 100 to 600 meters depending on the occurring events. The HMM is capable of segmenting an ECS signal into turnouts, disturbances and common track areas as well as giving a classification of the driving direction. This allows to distinguish between passing the turnout facing or trailing, which is essential to determine the starting point of the turnout. A typical result of the segmentation algorithm for a station on the test track is depicted in Figure 5. The red boxes indicate the segmented areas. The height represents their type and in case of a turnout also the driving direction. Further details on signal preprocessing, turnout modeling and segmentation are given in [16]. For Verification, 26 test

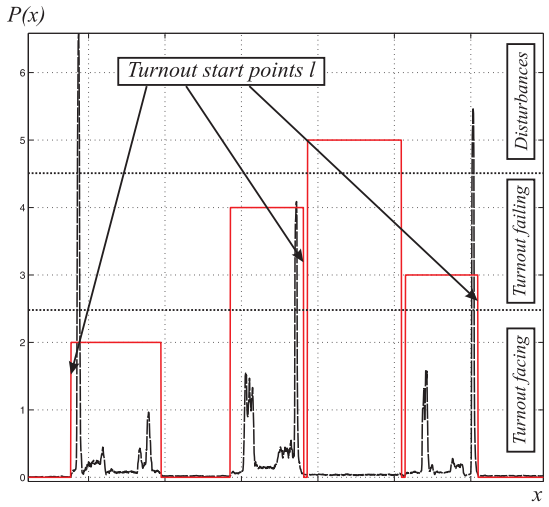

Fig. 5. Turnout segmentation and classification in passing facing or trailing. Observation sequence is the envelope of the power signal of $s(x)$.

drives on a real side track were done. An overall of 845 true turnout events are present in the signal, of which 831 were detected given only one false positive. Evaluation of the driving direction preclassification in the detection step lead to the following confusion matrix in Table I. The overall

TABLE I
CONFUSION MATRIX FOR HMM DETECTION RESULTS

Predicted	Turnout	No turnout	Facing	Failing
Turnout	831	14	-	-
No Turnout	1	∞	-	-
Turnout Facing	-	-	409	24
Turnout Failing	-	-	33	365

recognition rate is 98.23% for solely detection. From the 831 properly detected turnouts 774 were positively classified in the correct driving direction when distinguished in facing and failing what corresponds to a true positive rate of 93.14%.

C. Turnout Classification

The extracted signal samples are associated to a specific turnout and transformed in a new feature space for classification. Best results are achieved with wavelet transformed spatial signals (for details see [9]), of which three scales are taken. This results in a feature vector for every detected turnout that represents an observation sequence $\boldsymbol{\mathcal{O}}_j$ for the second HMM stage. Given J passings for a turnout one can assign $\boldsymbol{\mathcal{O}}_J^m$ sequences to an according HMM $\boldsymbol{\Lambda}_m$, with $m = 1...M$ and $M = 4 \cdot \mathcal{M}$ for $\mathcal{M}$ turnouts. In this notation is each driving direction of a turnout represented by a single HMM. The models are trained with a modified Baum-Welch algorithm for multiple training sequences and Gaussian mixture models for the emissions (details in [14]). The classification is based on the log-likelihood computed with the common forward algorithm. After an initial manual association all new classified sequences $\boldsymbol{\mathcal{O}}_j^m$ for a turnout m are used as training samples for further off-line refining of the model. This allows an adaptive response to slow changes in the ECS, e.g. phase angle shifts or deterioration (see [12]). The classifier performance was verified with real data from a side track that contains a medium amount of $\mathcal{M} = 14$ turnouts, resulting in $m = 34$ classes since not every turnout was crossed in every direction.

The overall error is computed on the test and validation sets that contain 277 turnout detections, taken from the overall segmented results in III-B. One *false positive* results in an classification performance of 99.64%. The HMM classification is robust up to a velocity estimation error (corresponding to a distortion of the signal) of 15%. It is also nonsensitive against possible cutting offs at the beginning or end of turnouts, that can occur in the detection HMM stage. A cut up to 3m from the switchblade area and up to 7m from the tail only slightly reduces performance to 99.28%, corresponding to two errors out of 277.

IV. Localization in Topological Maps

Rail vehicles are not steerable and can be modeled with one degree of freedom preset by the rail network. Turnouts represent exceptions for this assumption if driven over facing. It is therefore sufficient to know the current track segment and the position on it to realize a train localization. The sleeper count estimate $n_{\text{sl}}(t)$ described in Section II and the turnout extraction outlined in (Section III) are sufficient to solve this task. We combine them in topological maps which are a natural choice to represent a rail network. We assume a map in which the connections between nodes are known a priori. The number of sleepers between every two distinct locations are estimated from data. This assumptions allow to create a map out of very rough knowledge. Although we imply that the positioning can be done solely based on the ECS system, the probabilistic framework allows for an easy enhancement with additional sensors for landmark or feature detection, e.g. vision systems.

A. Map representation

Topological maps are a graph based abstract representation of the environment. They are an adequate choice for the given application due to their intuitive understanding, the scalability, and compact representation. We interpret the turnouts as vertices V and the connecting rail tracks as edges R in a graph. Figure 6 displays a map commonly present in signalling centers and trains. It contains all necessary information of the turnout connections and is enhanced with track specific features, such as road crossings or platform positions. The storage of the average sleeper distance Δn_i of rail segment R^i within the map (this can be done at every 100 m of a segment for inter station segments and 10 m within a station) allows a rough estimate of traveled distance in meters, if a comparison or fusion with other metrical distance sensors is needed. The relative position on a track element R^i is measured by the actual sleeper count divided by the number of sleepers between two turnouts that is stored within the map according to $x_{\text{rel}} = \frac{n_{\text{sl}}(t)}{n_{\text{sl}}^i}$.

For an internal representation in the positioning system, the map in Figure 6 is first transformed into a directed graph represented by the adjacency matrix G. In addition, each turnout $\mathcal{T}_s$ with $s = 1...\mathcal{M}$ can be driven over in four directions, and is thus associated with four HMMs $\boldsymbol{\Lambda}_m$ where for convenience $m = s, i$ with $i = 1..4$. The mapping and association is depicted in detail in Figure 7. The nodes V

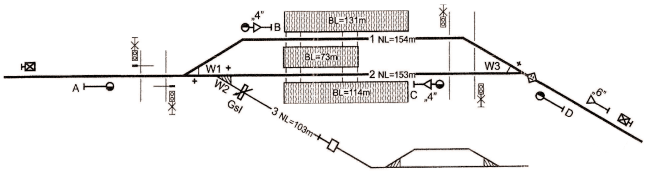

Fig. 6. Topological representation of a railway station on a side track.

and edges R are augmented with additional information, such as turnout coordinates for visualization purposes or special features such as the sleeper number.

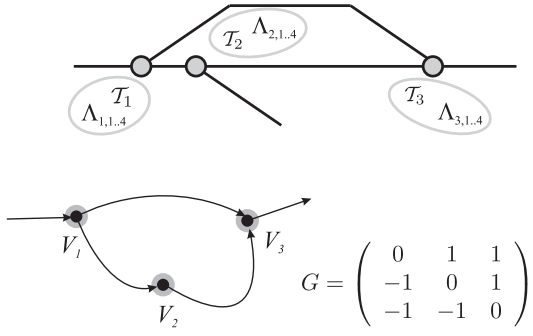

Fig. 7. Association of HMMs to specific turnouts and transformation of given map from Figure 6 into graph representation.

B. Probabilistic Recursive Positioning

The final localization of the rail vehicle is done in two parallel threads. The first continuously counts $n_{\text{sl}}(t)$ as described in Section II-A, resetting the counter to zero after any turnout detected by the first HMM stage.

The second thread associates a probability for being on a distinctive track segment R^i. This results in a multimodal location probability. The conditional a posteriori probability $P(R^i|S)$ of being on track segment R^i given sensor information S allows an augmentation to N independent information sources. Each source S^n with $n = 1..N$ is assumed independent what results in

$$P(S^1, S^2, ..., S^N|R^i) = \prod_{n=1}^{N} P(S^n|R^i). \tag{2}$$

If (2) holds, the a posteriori probability $P(R^i_{k+1}|\mathbf{S_k}, S_{k+1})$ for the next step, where $\mathbf{S_k} = S_1, ..., S_k$, can be rearranged to a recursive Bayesian update

$$P\left(R^i_{k+1}|S_{k+1}\right) = \frac{P\left(S_{k+1}|R^i_{k+1}\right) P\left(R^i_k\right)}{\sum_i \left[P\left(S_{k+1}|R^i_{k+1}\right) P\left(R^i_k\right)\right]}, \tag{3}$$

with the a priori probability $P(R^i_k) = P(R^i_k|S_k)$, as described in [17]. The subsequent steps k represent the discrete distance in multitudes of Δn_i and with 1 follows $k = \hat{d}_{\text{sl}}(t)$. The overall likelihood $\mathcal{L}^i(k)$ for being on track segment R^i at the distance k becomes with (2)

$$\mathcal{L}^i(k) = P\left(S_k|R^i_k\right) = \prod_{n=1}^{N} P(S^n_k|R^i_k), \tag{4}$$

where $P(S^n|R^i)$ is the likelihood of a single sensor n for hypothesis R^i.

Thus, the relative rail vehicle position on each segment follows from its particular probability $P(R^i_k|S_k)$ conditioned on the current distance k. The most probable vehicle position is calculated with a *maximum a posteriori (MAP)* estimate according to

$$R_{\text{MAP}}(k) = \underset{i}{\operatorname{argmax}}\, P(R^i_k|S^i_k), \tag{5}$$

given the posterior from (3).

C. Experimental Results

The proposed localization procedure was verified with real data from test drives with a common non-autonomous rail vehicle. The test track comprises a length of 18 km and 52 turnouts. Several test drives were performed spanning 11 turnouts and $i = 17$ rail segments R^i. The ECS was exclusively used as sensor, but split up in four *virtual sensors* S^n with $n = 1...4$ each representing specific track features. Each feature is stored within the topological map, whereas the most important information, the number of sleepers n^i_{sl} for each edge in the graph is estimated first.

We assume the map structure to be known initially, without additional information. All detection results are separately evaluated for each test drive j off-line. Each spatial signal $s(x)$ can afterwards be evaluated between two nodes by using the time indexed detection event of the HMM. We apply an *iterative reweighted least squares (IRLS)* as in [18] to robustly determine n^i_{sl}. Table II displays exemplary results for open track areas with mainly sleepers and segments in stations, where vehicles stand still and heavy disturbances induced by infrastructure are present. Working sites or deterioration of the ECS could lead to a constant offset in the detection windows or change the track geometry. Therefore, the sleeper count is always estimated off-line, based on the ten latest drives to realize an adaptive behavior. The repeat accuracy on open tracks is up to $\approx 0.2‰$ and significantly outperforms integrative distance measures that comprise an average error of approx. 0.8%. Table III compares the common onboard velocity and distance sensors, whereby the GPS distance is calculated by velocity integration. Approximate values were estimated by test drives, radar system values given by manufacturer. The advantage of discrete localization diminishes in stations, where the average counting error is $\approx 0.8\%$, with a minimum error quantized to $\epsilon_{min} = \Delta n_{\text{sl}} \approx 0.65$m. The relative position estimate for each rail segment is combined with the edge probability, that consists of four features:

TABLE II
ESTIMATE OF NUMBER OF SLEEPERS

Edge R^i	$\hat{n}_{\text{sl}}$	$\hat{\sigma}_{\hat{n}}$	length [m]
Open track 1	4379.37	2.0	≈ 2890
Open track 2	3973.57	4.65	≈ 2620
Within station 21	391.21	1.79	≈ 260
Within station 2	442.25	2.76	≈ 290

TABLE III
COMPARISON OF DIFFERENT DISTANCE SENSORS

Type	Stations ($100\,m$)	Open track ($3000\,m$)
Odometer	$\approx 2\,\%$	$\approx 2\,\%$
GPS	$\approx 2\,\%$	$\approx 0.8\,\%$
Radar	$1.5\,\%$	$1\,\%$
ECS	$\approx 2-4\,\%$	$\approx 0,5-1,5\,\%$
Sleeper count	$\approx 1-2\,\%$	$0.01\,\%-0.2\,\%$

S^1 is assumed to determine the average clamp distance within a specific interval of 25 sleepers.

S^2 evaluates the current sleeper count $n^i_{\text{sl}}(k)$ with the number of estimated sleepers $\hat{n}^i_{\text{sl}}$.

S^3 calculates the average signal power $P_s(k)$

$$P_s(x_0) = \frac{1}{I} \int_{x_0-I}^{x_0} s^2(x)\; dx, \tag{6}$$

within the interval I and $x_0 = \hat{d}_{\text{sl}}(t)$.

S^4 applies the signal power on a larger interval to calculate the distance to map-stored power signatures via *correlation optimized warping (COW)* [19], a dynamic programming approach for pattern recognition, that augments the well known *dynamic time warping* and is based on a correlative measure that better fits the ECS signals. The initial rail

segment association is either uniform or depending on the last known position. The probabilities for entering a new segment R^i are updated after a turnout detection, based on the classification result and prior probabilities of the recursive update. A likelihood probability function is designed for each sensor S^n and the recursive MAP estimate evaluated as described in Section IV-B. This allows a sequential edge hypothesis update at non specific intervals. Figure 8 shows results for a station, comprising of five possible rail segments R^i. An additional rejection hypothesis H^0 allows a validation

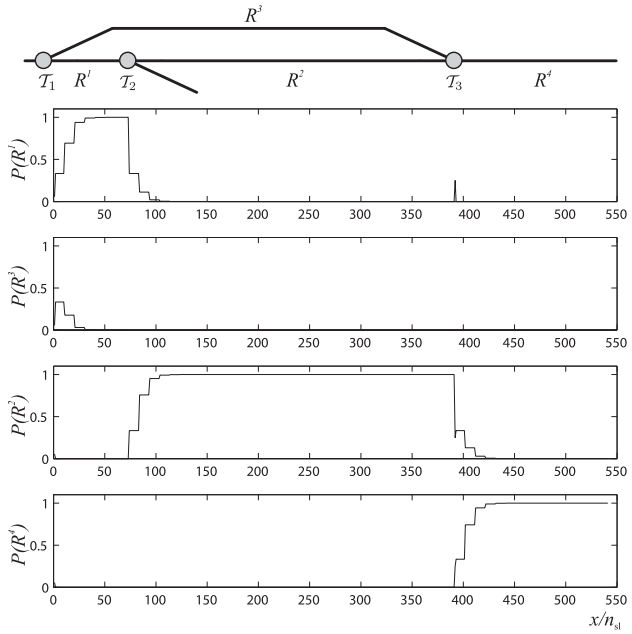

Fig. 8. Recursive edge hypothesis update for real data when crossing the station from Figure 6 (driving direction from left to right).

of the current position estimates and adds robustness against wrong detections. An undetected turnout or misclassified driving direction results in a significant rise of the rejection hypothesis and a new initialization with uniform prior on all hypothesis is applied. Figure 9 displays the efficiency of the validation step for a simulated non-detection of a turnout.

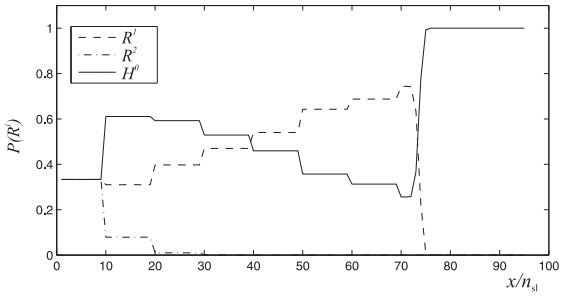

Fig. 9. Increase of the rejection probability H^0 after uniform initialization and a not detected turnout at sleeper position $n_{\mathrm{sl}} = 73$.

V. CONCLUSIONS

This contribution describes a novel approach for the localization of railroad vehicles. This is prerequisite for any autonomous applications in logistics or passenger transport. The combination of a discrete sleeper count algorithm, turnout detection, turnout classification and track segment identification allows a localization solely based on a novel eddy current sensor. Our approach is robust against wrong classification and detection, proves robust against hard environment conditions that appear in railway applications and outperforms commonly used distance sensors especially on longer track segments. the localization system was verified with real data recorded on a side track near Karlsruhe.

Future work will examine the combination of the discrete localization presented in this paper with continuous approaches as presented in [9]. Although a relative and discrete position information is not easy to combine with absolute sensors such as GPS, it will be crucial to incorporate different sensor principles and fusion techniques to satisfy the security standards for autonomous personal transportation systems.

REFERENCES

[1] U. Eberl, "The automatic freight car," *Pictures of the Future The magazine for Research and Innovation*, vol. Fall 2002, pp. 54 – 55, 2002.

[2] C. Henke, N. Frhleke, and J. Bcker, "Advanced convoy control strategy for autonomously driven railway vehicles," in *Proceedings of the IEEE ITSC*, 2006.

[3] A. Albanese and L. Marradi, "The rune project: the integrity performances of gnss-based railway user navigation equipment," in *Proceedings of the ASME/IEEE Joint Rail Conference*, pp. 211 – 218, 2005.

[4] F. Böhringer and A. Geistler, "Comparison between different fusion approaches for train-borne location systems," in *Proceedings of the IEEE MFI*, (New York), pp. 267–272, IEEE, 2006.

[5] S. Thrun, W. Burgard, and D. Fox, *Probabilistic Robotics*. Cambridge: The MIT Press, 2005.

[6] B. Kuipers, "The spatial semantic hierarchy," *Artifical Intelligence*, vol. 119, no. 1-2, pp. 191 – 233, 2000.

[7] H. Shatkay and L. Kaelbling, "Learning topological maps with weak local odometric information," in *Proceedings of IJCAI-97*, pp. 920 – 929, 1997.

[8] A. Ranganathan, *Probabilistic Topological Maps*. PhD thesis, Georgia Institute of Technology, March 2008.

[9] S. Hensel and C. Hasberg, "Bayesian techniques for onboard train localization," in *Proc. of IEEE Workshop on Statistical Signal Processing*, 2009.

[10] Y. Bar-Shalom, *Multitarget/Multisensor Tracking: Applications and Advances*, vol. 3. Norwood: Artech House, 2000.

[11] C. Bishop, *Pattern Recognition and Machine Learning*. Information Science and Statistics, 2006.

[12] T. Engelberg and F. Mesch, "Eddy current sensor system for non-contact speed and distance measurement of rail vehicles," in *Computers in Railways VII*, pp. 1261–1270, WIT Press, 2000.

[13] T. Strauss, "Reliable estimation of train velocity based on eddy current sensor signals," Master's thesis, Universität Karlsruhe, 2009.

[14] Y. Ephraim and N. Merhav, "Hidden markov processes," *IEEE Transactions on Information Theory*, vol. 48, pp. 1518 – 1569, June 2002.

[15] L. Grafakos, *Classical and Modern Fourier Analysis*. Pearson Education, 2004.

[16] S. Hensel and C. Hasberg, "HMM based segmentation of continuous eddy current sensor signals," in *Proc. IEEE International Conference on Intelligent Transportation Systems*, pp. 760 – 765, 2008.

[17] J. Pearl, *Probabilistic Reasoning in Intelligent Systems: Networks of plausible Inference*. Morgan Kaufmann Publishers, Inc., San Mateo, CA, 1988.

[18] P. J. Rousseeuw and A. M. Leroy, *Robust regression and outlier detection*. John Wiley & Sons, Inc., New York, NY, USA, 1987.

[19] G. Tomasi, F. van den Bergand, and C. Andersson, "Correlation optimized warping and dynamic time warping as preprocessing methods for chromatographic data," *Journal of Chemometrics*, vol. 18, pp. 231 – 241, 2004.